Journal of Statistical Mechanics:
Theory and Experiment

SISSA

PAPER: QUANTUM STATISTICAL PHYSICS, CONDENSED MATTER, INTEGRABLE SYSTEMS

Entanglement after quantum quenches in Lifshitz scalar theories

Journal of Statistical Mechanics: Theory and Experiment
An IOP and SISSA journal

PAPER: Quantum statistical physics, condensed matter, integrable systems

Entanglement after quantum quenches in Lifshitz scalar theories

Keun-Young Kim[1], Mitsuhiro Nishida[1], Masahiro Nozaki[2,3], Minsik Seo[1], Yuji Sugimoto[4] and Akio Tomiya[5]

[1] School of Physics and Chemistry, Gwangju Institute of Science and Technology, Gwangju 61005, Republic of Korea
[2] iTHEMS Program, RIKEN, Wako, Saitama 351-0198, Japan
[3] Berkeley Center for Theoretical Physics, Department of Physics, University of California, Berkeley, CA 94720, United States of America
[4] Interdisciplinary Center for Theoretical Study, University of Science and Technology of China, Hefei, Anhui 230026, People's Republic of China
[5] RIKEN/BNL Research center, Brookhaven National Laboratory, Upton, NY, 11973, United States of America
E-mail: fortoe@gist.ac.kr, mnishida@gist.ac.kr, masahiro.nozaki@riken.jp, tjalstlr23@gist.ac.kr, sugimoto@ustc.edu.cn and akio.tomiya@riken.jp

Received 11 July 2019
Accepted for publication 2 September 2019
Published 25 September 2019

Online at stacks.iop.org/JSTAT/2019/093104
https://doi.org/10.1088/1742-5468/ab417f

Abstract. We study the time evolution of the entanglement entropy after quantum quenches in Lifshitz free scalar theories, with the dynamical exponent $z > 1$, by using the correlator method. For quantum quenches we consider two types of time-dependent mass functions: end-critical-protocol (ECP) and cis-critical-protocol (CCP). In both cases, at early times the entanglement entropy is independent of the subsystem size. After a critical time (t_c), the entanglement entropy starts depending on the subsystem size significantly. This critical time t_c for $z = 1$ in the fast ECP and CCP has been explained well by the fast quasi-particle of the quasi-particle picture. However, we find that for $z > 1$ this explanation does not work and t_c is delayed. We explain why t_c is delayed for $z > 1$ based on the quasiparticle picture: in essence, it is due to the competition between the fast and slow quasiparticles. At late times, in the ECP, the entanglement entropy slowly increases while, in the CCP, it is oscillating with a well defined period by the final mass scale, independently of z. We give an interpretation of this phenomena by the correlator method. As

1742-5468/19/093104+27$33.00

z increases, the entanglement entropy increases, which can be understood by long-range interactions due to z.

Keywords: entanglement entropies, AdS/CFT correspondence

Contents

1. Introduction

Time evolution of non-equilibrium systems is an important subject in physics such as thermalization processes of quantum many body systems and black hole formation (see reviews [1, 2]). One well-studied protocol to describe the time evolution process of non-equilibrium systems is the quantum quench with a time dependent Hamiltonian (see for example [3–5] and figure 1 in this paper). In this case, one can calculate time evolution of the system and obtain insights on the time evolution through a measure of entanglement.

Typical choices of the time-dependent mass potentials are the ones in the end-critical-protocol (ECP) and cis-critical-protocol (CCP) [6]. In the ECP, the mass potential is nonzero at early times and approaches to zero at late times as shown in figure 1(a). On the other hand, in the CCP, the mass potential is nonzero at $t \to \pm\infty$ and becomes zero at $t = 0$ as shown in figure 1(b). The scaling property, the time evolution of correlation functions, entanglement measures, and complexity in the ECP and CCP were studied in [6–17].

When we consider the time evolution of a pure state due to a unitary time evolution operator, the density matrix cannot become a mixed state. However, the reduced density matrix of the total system can be the mixed states. After a sufficient time, this subsystem may show the properties of thermodynamic equilibrium. A measure to study these properties is the entanglement entropy, which is defined by von Neumann entropy for a reduced density matrix:

$$S_A = -\mathrm{Tr}_A \rho_A \log \rho_A, \tag{1.1}$$

where ρ_A is the reduced density matrix of the subsystem A. If the entanglement entropy S_A behaves as a thermodynamic entropy of an equilibrium state, one can interpret the subsystem A as thermodynamic equilibrium.

The time evolution of the entanglement entropy for an interval in two-dimensional conformal field theories (CFT) in a sudden quench, which is a protocol that the mass in the Hamiltonian is suddenly changed at $t = 0$, is well described by the quasiparticle picture (see, for example, [5, 18–20] and figure 6 in this paper). The basic idea is as follows: (i) by a sudden quench, the quasiparticle pairs are generated; (ii) these quasiparticles contribute to the change of entanglement entropy after the quench. For example, if the final mass after the quench is small enough, the maximum propagation speed of the quasiparticles is approximately the speed of light, so the entanglement entropy starts depending on subsystem size l from $t \sim \frac{l}{2}$ when l is large compared with the initial correlation length[6]. This result agrees with the analysis of two-dimensional

[6] This will be explained in more detail in section 3.3.

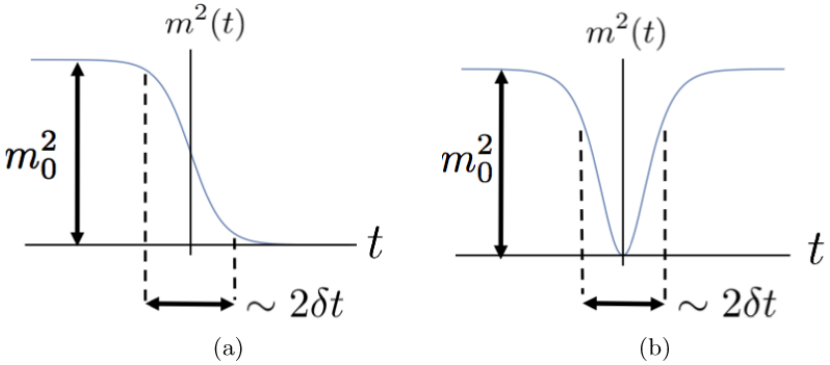

Figure 1. Schematic descriptions of the mass potential $m^2(t)$ in the ECP and the CCP. We will explain the ECP and CCP in more details in section 2. (a) End-critical-protocol (ECP). (b) Cis-critical-protocol (CCP).

CFT in a sudden quench. The quasiparticle formula in the sudden quench including the quasiparticles with various group velocities was studied in [21, 22].

Instead of systems with the Lorentz symmetry, one can consider the Lifshitz symmetry [23], which is the symmetry under a transformation

$$t \to \lambda^z t, \quad x \to \lambda x, \tag{1.2}$$

where z is the dynamical exponent, and λ is a positive scaling factor. For example, the Lifshitz symmetry can occur at some critical points in condensed matter systems [24], and a quantum gravity model with the Lifshitz symmetry has been proposed in [25]. Since Lorentz invariance is broken, the propagation speed of the quasiparticles and the behavior of the entanglement entropy in Lifshitz theories may be different from the ones in Lorentz invariant theories. Thus, it is important to check such different behavior of the entanglement entropy with the Lifshitz symmetry. The entanglement entropy in the Lifshitz theories was studied by field-theoretical methods and holographic methods in, for example, [26–35]. The time-independent entanglement entropy in the Lifshitz free scalar theories was studied in [36–39], and the time dependent entanglement entropy in the sudden quench of the Lifshitz free scalar theories was studied in [40] with $z > 1$ and in [41] with $0 < z < 1$.

In this paper, we study the time-dependent entanglement entropy on Lifshitz free scalar theories with $z > 1$ in $1 + 1$ dimensional spacetime. We compute the entanglement entropy by a correlator method, which is a computation method for free theories, on one-dimensional spacial lattice [18, 42, 43]. In order to obtain a perspective of continuum field theories from the computations on the lattice, we will take a smaller mass than the inverse lattice spacing to suppress cutoff effects.

There is a related previous work on this topic in [40], where only the sudden quench was considered. Here, we consider the slow and fast ECP and the slow and fast CCP. The sudden quench case in [40] can be obtained by the very fast limit of the ECP in our analysis. Another difference from [40] is the mass scales. While [40] deals with the initial mass scale of order 1, here we consider a small mass scale compared with the lattice spacing since we are interested in the field theory limit.

We have found many interesting features on the dynamics of the entanglement entropy: some are independent of the subsystem size and some are independent of the

J. Stat. Mech. (2019) 093104

dynamical exponent z. For example, at early times, in both ECP and CCP, the entanglement entropy is independent of the subsystem size and, at late times, in the CCP the entanglement entropy is oscillating in time with a well defined period, independently of z. We will interpret such properties by the quasiparticle picture and the idea of the correlator method.

In particular, there is an interesting distinctive property for $z>1$ compared with $z=1$ case. It is about a critical time t_c that the entanglement entropy starts depending on the subsystem size significantly[7]. While t_c for $z=1$ in the fast ECP and CCP can be explained well only by the fast quasiparticles of the quasiparticle picture, we find that this explanation does not work for $z>1$ and t_c is delayed. We will interpret this by a careful investigation of the quasiparticle picture. Note that a similar delay has been observed in some spin chain models without the Lifshitz symmetry [21, 44].

The paper is organized as follows: in section 2 we review how to compute the entanglement entropy of the Lifshitz free scalar theories on one-dimensional lattice by the correlator method. In section 3 we compute the time evolution of the entanglement entropy for $z>1$ in the ECP and, in section 4, we do so in the CCP. In section 5 we study the quasiparticle formula in the sudden quench with $z=2$, by which we interpret our results in sections 3 and 4. We conclude in section 6.

2. Set up and method

In this section, we consider a Hamiltonian of free scalar Lifshitz theories on one-dimensional lattice. In order to study the time evolution of the entanglement entropy, we consider the end-critical-protocol (ECP) and cis-critical-protocol (CCP), where mass potentials depend on time smoothly. We also define fast and slow limits of the ECP and CCP by using the relation between parameters in the mass potentials. Then, we explain how to compute the time evolution of entanglement entropy by using the correlator method[8].

2.1. Hamiltonian and equation of Lifshitz free scalar theories

In this subsection, we introduce a Hamiltonian of Lifshitz free scalar theories on one-dimensional *lattice* based on [36, 37, 40]. Let us first start with a Hamiltonian of Lifshitz free scalar field theories in 1 spacial dimension[9]

$$\bar{H}(t)=\frac{1}{2}\int \mathrm{d}x\left[\pi^2+\bar{\alpha}^2\left(\partial_x^z\phi\right)^2+\bar{m}(t)^2\phi^2\right], \tag{2.1}$$

where the overbar indicates dimensionful observables, and $\bar{m}(t)$ is a mass potential which depends on t.

[7] This 'significantly' should be quantified properly. Here, we are more qualitative. It simply means it is observable from our numerical plot.

[8] In this paper we do not explain details of numerical calculations, which can be found in appendix D in the previous paper [13].

[9] Our convention is the same as one in [37]. In this paper, we consider $z\in\mathbb{Z}_{>0}$.

J. Stat. Mech. (2019) 093104

For numerical computations, we construct a Hamiltonian on one-dimensional lattice from (2.1). Let us consider N lattice sites on a one-dimensional circle[10] and discretize the system with a lattice spacing ϵ. Accordingly, by replacing $\int \mathrm{d}x \to \epsilon \sum_{l=0}^{N-1}$, $\phi \to q_l$, $\partial_x^z \phi \to \epsilon^{-z} \sum_{m=0}^{z} (-1)^{z+m} \binom{z}{m} q_{l+m-1}$, $\pi \to p_l/\epsilon$, $\bar{\alpha} \to \alpha \epsilon^{z-1}$, $\bar{m}(t) \to m(t)/\epsilon$, and $\bar{H}(t) \to H(t)/\epsilon$, we obtain a lattice Hamiltonian on a discretized circle:

$$H(t) = \frac{1}{2} \sum_{l=0}^{N-1} \left[p_l^2 + \alpha^2 \left(\sum_{m=0}^{z} (-1)^{z+m} \binom{z}{m} q_{l+m-1} \right)^2 + m(t)^2 q_l^2 \right], \tag{2.2}$$

where $\binom{z}{m} := \frac{z!}{(z-m)!m!}$ is the binomial coefficient. Note that, from here, all variables and parameters are dimensionless and dimensionful quantities are recovered by the lattice spacing ϵ.

To simplify the interaction between q_l in the Hamiltonian (2.2), we use the Fourier transformations[11]:

$$\begin{aligned} q_l &= \frac{1}{\sqrt{N}} \sum_{\kappa=-\frac{N-1}{2}}^{\frac{N-1}{2}} \mathrm{e}^{\mathrm{i}\frac{2\pi l\kappa}{N}} \tilde{q}_\kappa, \\ p_l &= \frac{1}{\sqrt{N}} \sum_{\kappa=-\frac{N-1}{2}}^{\frac{N-1}{2}} \mathrm{e}^{\mathrm{i}\frac{2\pi l\kappa}{N}} \tilde{p}_\kappa, \end{aligned} \tag{2.3}$$

and we obtain

$$H(t) = \frac{1}{2} \sum_{\kappa=-\frac{N-1}{2}}^{\frac{N-1}{2}} \left[\tilde{p}_\kappa^\dagger \tilde{p}_\kappa + \left(\alpha^2 \left(2 \sin\left(\frac{\pi\kappa}{N} \right) \right)^{2z} + m^2(t) \right) \tilde{q}_\kappa^\dagger \tilde{q}_\kappa \right]. \tag{2.4}$$

Throughout this paper, we take $\alpha = 1$ without loss of generality because results for other values of α can be obtained by rescaling $m(t)$ and time.

We expand $\tilde{q}_\kappa$ and $\tilde{p}_\kappa$ by a creation operator $a_k^\dagger$ and an annihilation operator a_k as

$$\begin{aligned} \tilde{q}_\kappa &= f_\kappa(t) a_\kappa + f_{-\kappa}^*(t) a_{-\kappa}^\dagger, \\ \tilde{p}_\kappa &= \dot{f}_\kappa(t) a_\kappa + \dot{f}_{-\kappa}^*(t) a_{-\kappa}^\dagger, \end{aligned} \tag{2.5}$$

and we quantize them by the canonical commutation relations $[\tilde{q}_\alpha, \tilde{p}_\beta] = i\delta_{\alpha,-\beta}$, $[a_\alpha, a_\beta^\dagger] = \delta_{\alpha,\beta}$, and $[\tilde{q}_\alpha, \tilde{q}_\beta] = [\tilde{p}_\alpha, \tilde{p}_\beta] = [a_\alpha, a_\beta] = [a_\alpha^\dagger, a_\beta^\dagger] = 0$. From the Heisenberg equations of (2.5) with (2.4), the equation of $f_k(t)$ yields

$$\begin{aligned} &\frac{\mathrm{d}^2 f_k(t)}{\mathrm{d}t^2} + \omega_k^2(t)\, f_k(t) = 0, \\ &\omega_k(t) = \sqrt{\left(2 \sin\left(\frac{k}{2} \right) \right)^{2z} + m^2(t)}. \end{aligned} \tag{2.6}$$

[10] Here we impose the periodic boundary condition.

[11] We assume that N is an odd integer. One can also do the similar analysis with even N.

J. Stat. Mech. (2019) 093104

Here, we introduce the rescaled momentum k as

$$k := \frac{2\pi\kappa}{N}. \tag{2.7}$$

2.2. Two mass potentials: ECP and CCP

For numerical computations, we use smooth[12] mass potentials in which $f_k(t)$ has analytic solutions of (2.6). One of them is the mass potential in the end-critical-protocol (ECP) [6]:

$$m^2(t) = \frac{m_0^2}{2}\left[1 - \tanh\left(\frac{t}{\delta t}\right)\right]. \tag{2.8}$$

In the ECP, the initial mass is m_0, and the mass potential decreases with time and becomes zero at late times as shown in the left panel of figure 1. Another mass potential with which we can obtain an analytic solution of (2.6) is the mass potential in the cis-critical-protocol (CCP) [6]:

$$m^2(t) = m_0^2 \tanh^2\left(\frac{t}{\delta t}\right). \tag{2.9}$$

In the CCP, the initial and final masses are m_0, and the mass potential at $t = 0$ becomes zero as shown in the right panel of figure 1.

An explicit solution of (2.6) in the ECP is [45],

$$\begin{aligned} f_k(t) =& \frac{1}{\sqrt{-4i\beta/\delta t}}\left(\frac{1+\tanh[t/\delta t]}{2}\right)^{-\beta}\left(\frac{1-\tanh[t/\delta t]}{2}\right)^{-\alpha} \\ & \times\ {}_2F_1(-\alpha-\beta+1, -\alpha-\beta; -2\beta+1; (1+\tanh[t/\delta t])/2), \\ \alpha :=& -\frac{\mathrm{i}\delta t}{2}|2\sin[k/2]|^z,\ \ \beta := \frac{\mathrm{i}\delta t}{2}\sqrt{(2\sin[k/2])^{2z}+m_0^2}, \end{aligned} \tag{2.10}$$

and one in the CCP is [8],

$$\begin{aligned} f_k(t) =& \frac{2^{\mathrm{i}\omega_0\delta t}}{\sqrt{2\omega_0}}\frac{(\cosh[t/\delta t])^{2\alpha}}{E_{1/2}E'_{3/2}-E_{3/2}E'_{1/2}} \times \left[E'_{3/2}\ {}_2F_1\left(a, b; \frac{1}{2}; -\sinh^2[t/\delta t]\right)\right. \\ & \left. + E'_{1/2}\sinh[t/\delta t]{}_2F_1\left(a+\frac{1}{2}, b+\frac{1}{2}; \frac{3}{2}; -\sinh^2[t/\delta t]\right)\right], \\ & a := \alpha - \frac{\mathrm{i}\omega_0\delta t}{2},\ \ b := \alpha + \frac{\mathrm{i}\omega_0\delta t}{2}, \\ & \alpha := \frac{1+\sqrt{1-4(m_0\delta t)^2}}{4},\ \ \omega_0^2 := (2\sin[k/2])^{2z}+m_0^2, \\ & E_{1/2} := \frac{\Gamma(1/2)\Gamma(b-a)}{\Gamma(b)\Gamma(1/2-a)},\ \ E_{3/2} := \frac{\Gamma(3/2)\Gamma(b-a)}{\Gamma(1/2+b)\Gamma(1-a)},\ \ E'_c := E_c(a \leftrightarrow b). \end{aligned} \tag{2.11}$$

[12] Contrary to 'smooth', we may consider the 'sudden' quench, which is realized by a step function.

J. Stat. Mech. (2019) 093104

2.3. Fast and slow limits

The mass potentials (2.8) and (2.9) depend on m_0 and δt, where we define an initial ($t \to -\infty$) length scale ξ as $\xi := 1/m_0$. By using these parameters, we define two limits of the quenches as in [10]: fast and slow limits. The fast limit is defined such that δt is much smaller than the initial length scale ξ, i.e.

$$\delta t \ll \xi, \tag{2.12}$$

while the slow limit is defined such that δt is much larger than the initial length scale ξ as

$$\delta t \gg \xi. \tag{2.13}$$

One characteristic difference between the fast and slow limit is time scales when the adiabaticity breaks. To define the time scale, we use a dimensionless function

$$C_{\rm L}(t) := \left| \frac{1}{m^2(t)} \times \frac{{\rm d}m(t)}{{\rm d}t} \right| \tag{2.14}$$

for a criteria of the adiabaticity (Landau criteria). See [10, 16, 46], for details. If $C_{\rm L}(t)$ satisfies $C_{\rm L}(t) \ll 1$, we can use the adiabatic expansion because the adiabaticity is held. The Kibble–Zurek time $t_{\rm kz}$[13] is defined such that

$$C_{\rm L}(t_{\rm kz}) \sim 1, \tag{2.15}$$

which means that $t_{\rm kz}$ is the time scale when the adiabaticity starts breaking (or being restored in the case of CCP).

In the fast limit $t_{\rm kz} \sim 0$, while $t_{\rm kz}$ in the slow limit is far from $t = 0$. The Kibble–Zurek time $t_{\rm kz}$ in the slow ECP and CCP is [10]

$$t_{\rm kz} \sim \delta t \log[\delta t/\xi] \quad ({\rm ECP}), \tag{2.16}$$

$$t_{\rm kz} \sim (\delta t \xi)^{\frac{1}{2}} \quad ({\rm CCP}). \tag{2.17}$$

In the slow ECP, the adiabaticity is broken after $t \sim t_{\rm kz}$, and the one in the slow CCP is broken from $t \sim -t_{\rm kz}$ to $t \sim t_{\rm kz}$. For later use, we here define a length scale $\xi_{\rm kz}$ at $t = t_{\rm kz}$ as

$$\xi_{\rm kz} := \frac{1}{m(t_{\rm kz})} \sim \delta t \quad ({\rm ECP}), \tag{2.18}$$

$$\xi_{\rm kz} := \frac{1}{m(t_{\rm kz})} \sim (\delta t \xi)^{\frac{1}{2}}, \quad ({\rm CCP}). \tag{2.19}$$

2.4. Correlator method

In free scalar theories, we can compute the entanglement entropy by using two-point functions. This computation method is called as the correlator method [18, 42, 43], and here we review this method based on [47].

[13] This $t_{\rm kz}$ is determined from $\omega_k(t)$ at $k = 0$. See section 3 in [16] for more detail.

J. Stat. Mech. (2019) 093104

In our computations, we consider a thermodynamic limit $N \to \infty$ with fixed ϵ. In this limit, (2.3) is written as

$$q_l(t) := \int_{-\pi}^{\pi} \frac{\mathrm{d}k}{\sqrt{2\pi}} \tilde{q}_k \mathrm{e}^{\mathrm{i}kl}, \tag{2.20}$$

$$p_l(t) := \int_{-\pi}^{\pi} \frac{\mathrm{d}k}{\sqrt{2\pi}} \tilde{p}_k \mathrm{e}^{\mathrm{i}kl}, \tag{2.21}$$

and two-point functions of $q_l(t)$ and $p_l(t)$ are

$$Q_{ab}(t) := \langle 0|q_a(t)q_b(t)|0\rangle = \int_{-\pi}^{\pi} \frac{\mathrm{d}k}{2\pi} |f_k(t)|^2 \cos\left(k\,|a-b|\right), \tag{2.22}$$

$$P_{ab}(t) := \langle 0|p_a(t)\,p_b(t)|0\rangle = \int_{-\pi}^{\pi} \frac{\mathrm{d}k}{2\pi} \left|\dot{f}_k(t)\right|^2 \cos\left(k\,|a-b|\right), \tag{2.23}$$

$$D_{ab}(t) := \frac{1}{2}\,\langle 0|\,\{q_a(t), p_b(t)\}\,|0\rangle = \int_{-\pi}^{\pi} \frac{\mathrm{d}k}{2\pi} \mathrm{Re}\left[\dot{f}_k^*(t)\,f_k(t)\right] \cos\left(k\,|a-b|\right), \tag{2.24}$$

where $|0\rangle$ is the ground state for the initial Hamiltonian. With the explicit expressions of $f_k(t)$ in the ECP (2.10) and the CCP (2.11), these two-point functions can be computed numerically.

In the correlator method, the entanglement entropy of the subsystem A with the number of lattice sites l can be computed by the eigenvalues of a matrix $\mathcal{M}$ constructed from the two point functions,

$$\mathcal{M} := \mathrm{i}J\Gamma, \quad J := \begin{bmatrix} 0 & I_{l\times l} \\ -I_{l\times l} & 0 \end{bmatrix}, \quad \Gamma := \begin{bmatrix} Q_{ab}(t) & D_{ab}(t) \\ D_{ab}(t) & P_{ab}(t) \end{bmatrix}, \tag{2.25}$$

where $I_{l\times l}$ is an $l \times l$ unit matrix. By computing positive eigenvalues of the $2l \times 2l$ matrix $\mathcal{M}$, say γ_a, we obtain the entanglement entropy $S_A(t)$ for a subsystem A as follows:

$$S_A(t) = \sum_{a=1}^{l} \left[\left(\gamma_a + \frac{1}{2}\right)\log\left(\gamma_a + \frac{1}{2}\right) - \left(\gamma_a - \frac{1}{2}\right)\log\left(\gamma_a - \frac{1}{2}\right)\right]. \tag{2.26}$$

In this paper, we study the time evolution of the entanglement entropy in the free Lifshitz scalar theories. In order to study the time evolution, we compute a change of the entanglement entropy

$$\Delta S_A(t) = S_A(t) - S_A(-\infty). \tag{2.27}$$

In particular, we investigate z-dependence and l-dependence of ΔS_A.

3. Entanglement entropy in the ECP with $z > 1$

In this section, we first describe our numerical results on the time evolution of the entanglement entropy in the fast and slow ECP. After that, we provide interpretations of our results.

J. Stat. Mech. (2019) 093104

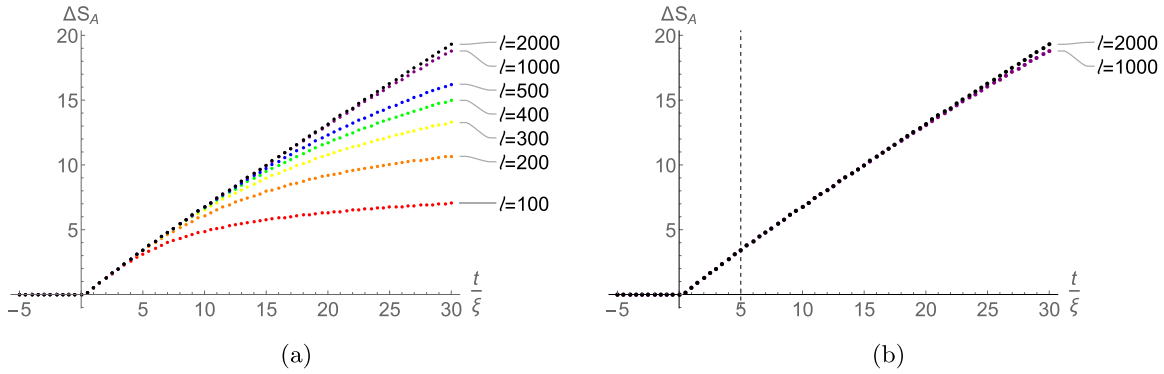

Figure 2. Time dependence of ΔS_A in the fast ECP for $z=2$ ($\xi=100, \delta t=5$). (a) Comparison between different subsystem sizes l. (b) Comparison between $l=1000, 2000$. The dashed line designates the critical time for $z=1$: $\frac{t_c}{\xi} \sim \frac{l}{2\xi} = 5$ for $l=1000$.

3.1. Fast ECP

As an example of the fast ($\delta t/\xi \ll 1$) ECP with $z \neq 1$ (Lifshitz theory), we choose

$$\xi = 100, \quad \delta t = 5. \tag{3.1}$$

Figure 2 shows l-dependence of ΔS_A for $z=2$ with $l=100, 200, 300, 400, 500, 1000, 2000$. The entanglement entropy in the fast ECP with small $\delta t/\xi$ is similar to one in the sudden quench because the sudden quench is expected to be a limit of the ECP with $\delta t \to 0$. We observe the following properties from figure 2:

(Ef1) The change of the entanglement entropy ΔS_A begins to increase around $t \sim 0$ like the sudden quench case.

(Ef2) At early times, all plots lie on the same curve independently of the subsystem size l. It means ΔS_A has no subsystem size-dependence at early times.

(Ef3) At late times, ΔS_A with the different subsystem sizes is different. The critical time t_c, when the significant subsystem size-dependence of ΔS_A occurs, increases with the subsystem size. For $z=1$, it is expected that $t_c(z=1) \sim l/2$ from the quasiparticle picture [13]. For $z=2$, we find $t_c(z=2) > t_c(z=1)$. For example, see figure 2(b), where $t_c(z=1)/\xi \sim 5$, while $t_c(z=2)/\xi \sim 25$ for $l=1000$.

Figure 3 shows z-dependence of ΔS_A for $l=2000$ with $z=2, 4, 6, 8$. The change ΔS_A in this figure has the following properties of the z-dependence:

(Ef4) As z increases, ΔS_A also increases.

(Ef5) In the figure, we focus on the time range before l-dependence appears significantly. At late times, ΔS_A linearly increases with t, while ΔS_A at early times increases nonlinearly. This nonlinearity is sustained for a wide time range as z increases.

3.2. Slow ECP

As an example of the slow ($\delta t/\xi \gg 1$) ECP with $z \neq 1$ (Lifshitz theory), we choose

J. Stat. Mech. (2019) 093104

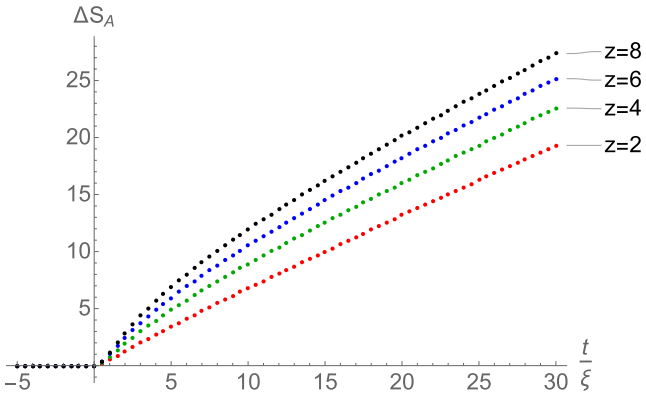

Figure 3. Time dependence of ΔS_A in the fast ECP with $\xi = 100, \delta t = 5, l = 2000$ and $z = 2, 4, 6, 8$.

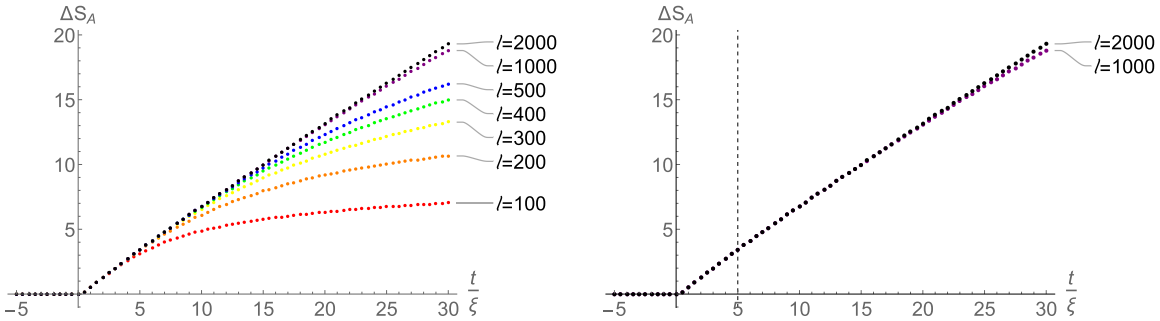

Figure 4. Time dependence of ΔS_A in the slow ECP for $z = 2$ ($\xi = 5, \delta t = 500$). (a) Comparison between different subsystem sizes l. (b) Comparison between $l = 1000, 2000$. The dashed line designates the critical time for $z = 1$: $\frac{t_c}{\delta t} \sim \frac{t_{\rm kz}}{\delta t} + \frac{l}{2\delta t} \sim 4.8$ for $l = 1000$ ($t_{\rm kz} \sim 2300$).

$$\xi = 5, \quad \delta t = 500. \tag{3.2}$$

Figure 4 shows l-dependence of ΔS_A for $z = 2$ with $l = 10, 50, 100, 300, 1000, 2000$. We observe the following properties from figure 4:

(Es1) The change ΔS_A in the slow ECP starts increasing at $t < 0$, unlike the fast or sudden quench cases.

(Es2) At early times ΔS_A has no subsystem size-dependence, like the fast ECP.

(Es3) At late times, ΔS_A with the different subsystem sizes are different and the critical time t_c increases with the subsystem size, like the fast ECP. For $z = 1$ and large l, it is expected that $t_c(z = 1) \sim t_{\rm kz} + l/2$ from the quasiparticle picture [13]. For $z = 2$, we find that $t_c(z = 2) > t_c(z = 1)$. For example, see figure 4(b), where $t_c(z = 1)/\delta t \sim 4.8$ ($t_{\rm kz} \sim 2300$ by (2.16) and $l = 1000$) while $t_c(z = 2)/\delta t > 10$.

Figure 5 shows z-dependence of ΔS_A for $l = 1000$ with $z = 2, 4, 6, 8$. The change ΔS_A in this figure has the following properties of the z-dependence:

J. Stat. Mech. (2019) 093104

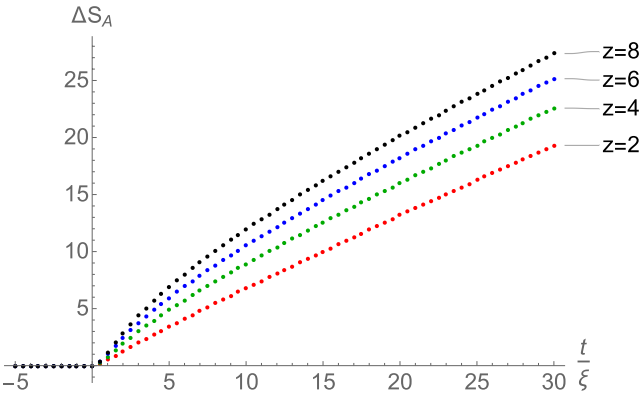

Figure 5. Time dependence of ΔS_A in the slow ECP with $\xi = 5, \delta t = 500, l = 1000$ and $z = 2, 4, 6, 8$.

(Es4) Like the fast ECP, ΔS_A increases as z becomes large.

(Es5) In the figure, we focus on the time range before l-dependence appears significantly. Like the fast ECP, ΔS_A increases nonlinearly, this nonlinearity is sustained for a wide time range as z increases.

3.3. Interpretation of the properties

In this subsection, we interpret the aforementioned properties of the entanglement entropy for the ECP.

3.3.1. (Ef1) and (Es1). The mass potential $m^2(t)$ starts decreasing around $t \sim -\delta t$. Therefore, ΔS_A in the slow ECP starts increasing at $t < 0$. For the fast ECP, however, since $\delta t \sim 0$, $m^2(t)$ starts decreasing around $t \sim 0$, and ΔS_A starts increasing around $t \sim 0$.

3.3.2. (Ef2) and (Es2). To understand the subsystem size-independence of ΔS_A at early times we use the quasiparticle picture [19, 21, 22]. To explain the quasiparticle picture, let us consider a one-dimensional system with a subsystem A of length l under a sudden quench, where the mass potential changes at $t = 0$ from the initial mass m_0 to the final mass $m_f = 0$. Due to a sudden quench at $t = 0$, the quasiparticle pairs are created at $t = 0$ everywhere and then propagate with the group velocity $v_k = \frac{\mathrm{d}\omega_k}{\mathrm{d}k}$ with the momentum k which is computed by the Hamiltonian after a quench.

As shown in figure 6, at the time t, only the quasiparticle pairs created in the yellow and green region will contribute to the entanglement entropy because one of the pairs is inside the subsystem A and the other is outside of A. In other words, the quasiparticle pairs created in the length of $2|v_k|t$ contribute in early time regime $t < \bar{t} := \frac{l}{2|v_k|}$ (yellow area in figure 6), while the quasiparticle pairs created in the length of l contribute in late time regime $t > \bar{t}$ (green area). Therefore, the entanglement entropy for the subsystem A, *generated by the quasiparticle pairs with the group velocity* v_k, depends on the subsystem size l of A after $t = \bar{t} = \frac{l}{2|v_k|}$ and does not depend on the subsystem size in early time regime $t < \bar{t}$. It turns out that this quasiparticle picture is consistent

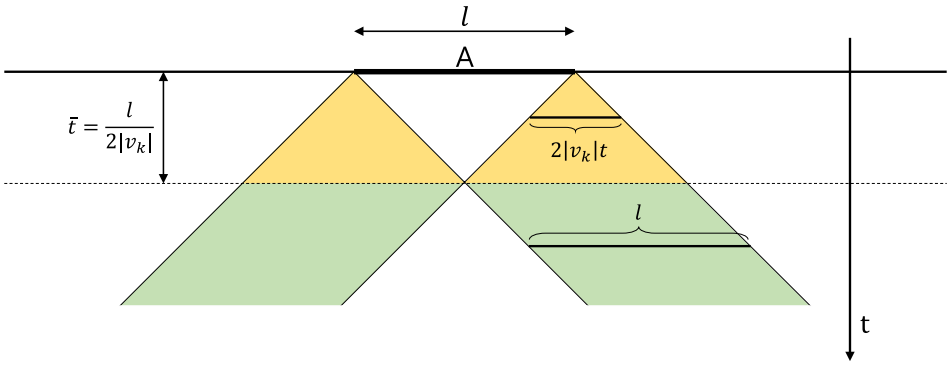

Figure 6. Quasiparticle picture in the sudden quench. The length of the subsystem A is l, and v_k is the group velocity of the quasiparticle pairs created at $t = 0$. In $t < \bar{t}$ the range of $2|v_k|t$ (yellow area) contributes to the entanglement entropy, while in $t > \bar{t}$ the range of l (green area) contributes to the entanglement entropy.

with the entanglement entropy with $z = 1$ in the two-dimensional CFT [19], the sudden quench [41], and the ECP [13].

3.3.3. (Ef3). In general, the group velocity v_k depends on the momentum k of the quasiparticle, thus we need to consider the quasiparticles with various velocities. In order to determine the critical time t_c, we may use the maximum group velocity $v_{\max}$,

$$t_c \sim \min\{\bar{t}\} = \frac{l}{2|v_{\max}|}, \tag{3.3}$$

because it is the earlist time the subsystem size dependence enters.

For example, since $v_{\max} = 1$ for the massless quasiparticle with $z = 1$, t_c with $z = 1$ becomes $t_c \sim \frac{l}{2}$ from (3.3), which is shown in figure 2(b). For $z > 1$, the maximum group velocity is $|v_{\max}| > 1$, so we expect t_c to obey $t_c < l/2$. However, figure 2(a) shows

$$t_c > \frac{l}{2} \qquad (z = 2). \tag{3.4}$$

We also confirmed this delayed t_c for $z = 4, 6, 8$.

One possible interpretation of this delayed t_c in the quasiparticle picture is as follows. The entanglement entropy by the quasiparticle pairs comes from not only the ones with the fast velocity close to $|v_{\max}|$, but also the sum of all quasiparticles with various v_k. If the contribution of the fast quasiparticles to ΔS_A can be suppressed compared with the slow quasiparticles, the subsystem size-dependence around $t_c \sim \frac{l}{2|v_{\max}|}$ for the fast ECP may be negligible. Thus, if this conjecture works, in more general, we expect t_c to satisfy

$$t_c \gg \frac{l}{2|v_{\max}|}, \tag{3.5}$$

where $t_c \gg \frac{l}{2|v_{\max}|}$ means that t_c is large enough so that we can observe difference between t_c and $\frac{l}{2|v_{\max}|}$ from numerical plots. Note that the condition (3.4) may not be satisfied even if (3.5) is satisfied because it is still possible, in principle,

J. Stat. Mech. (2019) 093104

$$\frac{l}{2|v_{\max}|} < t_c < \frac{l}{2}, \tag{3.6}$$

for $|v_{\max}| > 1$. In section 5, we show our conjecture works by using the quasiparticle formula in the sudden quench [21, 22].

3.3.4. (Es3). The quasiparticle picture is more applicable to the fast ECP rather than the slow ECP, because it is based on the sudden quench. However, we may slightly modify the argument by introducing the Kibble–Zurek time $t_{\rm kz}$ (2.16). The quasiparticles are generated not at $t \sim 0$ but at $t \sim t_{\rm kz}$ in the slow ECP with large l, thus t_c in the slow ECP with $z = 1$ from the fast quasiparticles is

$$t_c \sim t_{\rm kz} + \frac{l}{2} \qquad (z = 1), \tag{3.7}$$

as shown in figure 4(b). Indeed, it is confirmed by the correlator method in [13]. By the same argument as in the slow ECP case, we expect t_c to satisfy[14]

$$t_c \gg t_{\rm kz} + \frac{l}{2|v_{\max}|}, \tag{3.8}$$

for $z > 1$. Figure 4(b) is one of the examples[15]. We also confirmed this delayed t_c for $z = 4, 6, 8$.

3.3.5. (Ef4,5) and (Es4,5). The free Lifshitz scalar field theories with $z > 1$ have a higher spatial derivative interaction. After discretizing these field theories to lattice theories, this higher derivative interaction becomes a long-range interaction between the fields at two separate lattice points. As explained in [36, 37, 40], ΔS_A increases as z increases because of the long-range interaction (the properties (Ef4) and (Es4)). We suspect that the nonlinear increase of ΔS_A with t described in the properties (Ef5) and (Es5) is related to the large value of z, but we do not have a clear interpretation.

4. Entanglement entropy in the CCP with $z > 1$

In this section, we study the time evolution of entanglement entropy in the CCP with $z > 1$ and interpret its properties. Unlike ΔS_A in the ECP, ΔS_A in the CCP oscillates in time t because of the nonzero mass potential at late times.

[14] For $z = 1$ and large l, $t_{\rm kz} + \frac{l}{2|v_{\max}|}$ is a good criteria because both $t_{\rm kz}$ and $v_{\max}$ is evaluated at $k \sim 0$ [13, 16]. However, for $z \geqslant 2$, it may not because $t_{\rm kz}$ is determined from $\omega_k(t)$ at $k = 0$ while $v_{\max}$ is defined at finite k away from $k = 0$ as shown in figure 13. In principle, we have to find $k = \tilde{k}$ such that $t_{\rm kz}(\tilde{k}) + \frac{l}{2|v(\tilde{k})|}$ can be minimized and use it as a criteria. Here, $t_{\rm kz}(k)$ is the time scale when the adiabaticity of $\omega_k(t)$ starts breaking, of which precise meaning is shown in equation (3.10) in [16]. Note that in principle $t_{\rm kz}(k)$ can be defined for every k, but we used $t_{\rm kz} := t_{\rm kz}(0)$ for simplicity.

[15] As we noted in (3.6), it does not guarantee $t_c > t_{\rm kz} + \frac{l}{2}$. However, in our cases, it turns out to be true. See section 5.3 for more details.

J. Stat. Mech. (2019) 093104

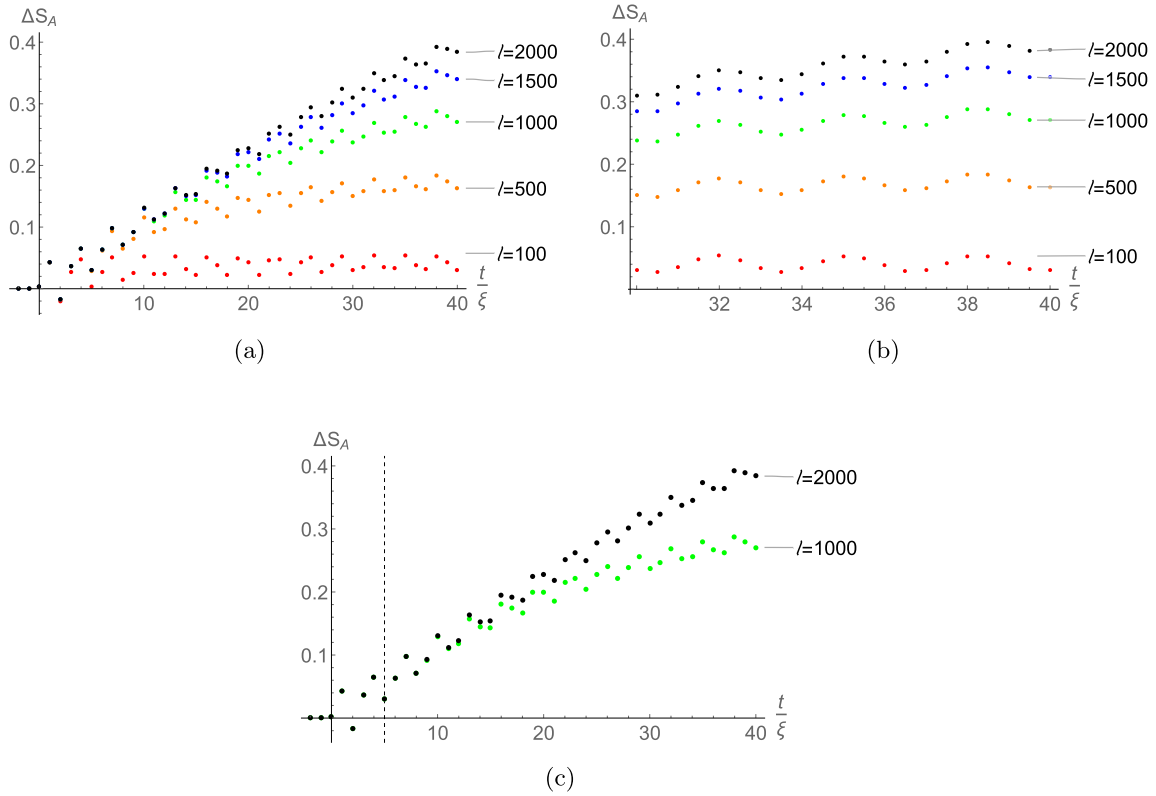

Figure 7. Time dependence of ΔS_A in the fast CCP for $z=2$ ($\xi=100, \delta t=5$). (a) Comparison between different subsystem sizes l ($-2\leqslant t/\xi\leqslant 40$). (b) Zoomed-in view of (a) ($30\leqslant t/\xi\leqslant 40$) to see the oscillating feature clearly. (c) Comparison between $l=1000, 2000$. The dashed line at $\frac{t}{\xi}=\frac{l}{2\xi}=5$ for $l=1000$ is shown for comparison with $z=1$.

4.1. Fast CCP

As an example of the fast ($\delta t/\xi \ll 1$) CCP with $z\neq 1$ (Lifshitz theory), we choose the same parameter as the fast ECP:

$$\xi=100, \quad \delta t=5. \tag{4.1}$$

Figure 7 shows l-dependence of ΔS_A for $z=2$ with $l=100, 500, 1000, 1500, 2000$. We observe the following properties from figure 7:

(Cf1) The change ΔS_A in the fast CCP starts increasing at $t\sim 0$ and oscillates with t. The period of the oscillation at late times is about $\pi\xi$. See figure 6(b). This period is the same as the case with $z=1$ [13].

(Cf2) The change ΔS_A is the global minimum around $t\sim 2\xi$ which is the same as the case with $z=1$ [13].

(Cf3) Like the slow and fast ECP, at early times ΔS_A has no subsystem size-dependence while at late times ΔS_A with the different subsystem sizes are different. Again, the critical time t_c increases with the subsystem size. For $z=1$, it was shown that

J. Stat. Mech. (2019) 093104

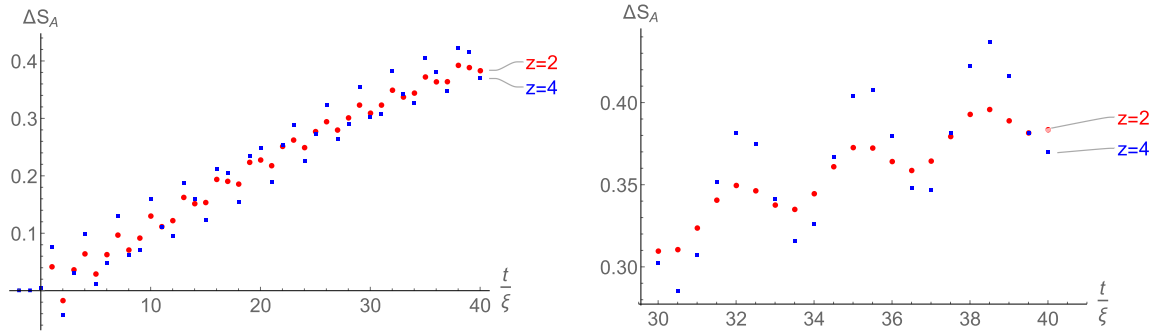

Figure 8. Time dependence of ΔS_A in the fast CCP with $\xi = 100, \delta t = 5, l = 2000$ and $z = 2, 4$. (a) Comparison between $z = 2, 4$ ($-2 \leqslant t/\xi \leqslant 40$). (b) Zoomed-in view of (a) ($30 \leqslant t/\xi \leqslant 40$) to see the oscillating feature clearly.

$t_c(z = 1) \sim l/2$ [13]. For $z = 2$, we find that $t_c(z = 2) > t_c(z = 1)$. For example, see figure 6(c), where $t_c(z = 1)/\xi \sim 5$, while $t_c(z = 2)/\xi > 10$ for $l = 1000$.

Figure 8 shows the dynamical exponent-dependence of ΔS_A for $l = 2000$ with $z = 2$ and 4[16]. The change ΔS_A in the fast CCP shows the following properties:

(Cf4) As z increases, the amplitude of oscillation in ΔS_A increases.
(Cf5) The period of oscillation ($\pi\xi$) and the time scale when ΔS_A is minimum ($t \sim 2\xi$) are independent of z.

4.2. Slow CCP

Next, as an example of the slow ($\delta t/\xi \gg 1$) CCP with $z \neq 1$ (Lifshitz theory), we choose[17]

$$\xi = 10, \quad \delta t = 1000. \tag{4.2}$$

Figure 9 shows the subsystem size l-dependence of ΔS_A for $z = 2$ with $l = 10, 50, 100, 200, 2000$. We observe the following properties in figure 9:

(Cs1) Unlike the fast CCP case, ΔS_A in the slow CCP with $z = 2$ starts increasing at $t < 0$ and oscillates with t. Like the fast CCP case, its period of oscillation at late times is about $\pi\xi$ which is the same as the case with $z = 1$ [13].

(Cs2) The change ΔS_A is first local minimum around $t \sim 2\xi_{kz}$ which is the same as the case with $z = 1$ [13].

[16] We plot ΔS_A with $z = 2, 4$ only because we need more precision for the numerical computation of ΔS_A in the fast CCP with large z to reduce the numerical error.
[17] In the slow CCP, we use the adiabatic approximation of $f_k(t)$ and its time derivative at large $|k|$ because the computational cost of evaluating the two point functions $Q_{ab}(t)$, $P_{ab}(t)$, and $D_{ab}(t)$ increases in the slow CCP. The approximation which we use in this paper is the same one used in [13, 16].

J. Stat. Mech. (2019) 093104

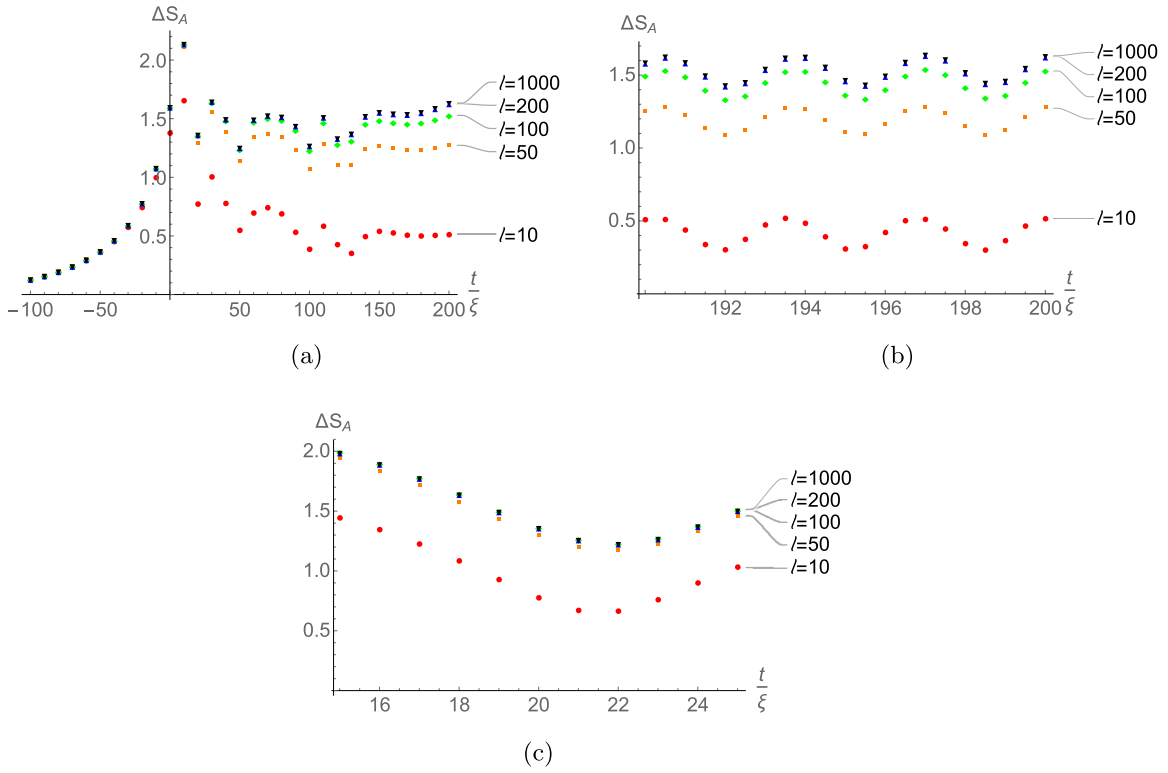

Figure 9. Time dependence of ΔS_A in the slow CCP for $z = 2$ ($\xi = 10, \delta t = 1000$). (a) Comparison between different subsystem sizes l ($-100 \leqslant t/\xi \leqslant 200$). (b) Zoomed-in view of (a) ($190 \leqslant t/\xi \leqslant 200$) to see the oscillating feature clearly. (c) Zoomed-in view of (a) ($15 \leqslant t/\xi \leqslant 25$) to see a local minimum around $t/\xi \sim 2\xi_{\rm kz}/\xi \sim 20$.

(Cs3) Like the slow/fast ECP and fast CCP, at early times ΔS_A has no subsystem size-dependence while, at late times ΔS_A with the different subsystem sizes are different. Again, the critical time t_c increases with the subsystem size.

Figure 10 shows the dynamical exponent-dependence of ΔS_A for $z = 2, 4, 6, 8$ with $l = 1000$. The change ΔS_A in the slow CCP shows the following properties:

(Cs4) Like the fast CCP, the amplitude of oscillation in ΔS_A becomes large when the dynamical exponent z increases.
(Cs5) Like the fast CCP, the period of oscillation ($\pi\xi$) and the time scale when ΔS_A is local minimum ($t \sim 2\xi_{\rm kz}$) are independent of z.

4.3. Interpretation of the properties

In this subsection, we interpret the aforementioned properties of the entanglement entropy for the CCP.

4.3.1. (Cf1,5) and (Cs1,5). Like ΔS_A in the ECP, ΔS_A in the fast CCP starts increasing from $t \sim 0$, while ΔS_A in the slow CCP starts increasing from $t < 0$ simply because

J. Stat. Mech. (2019) 093104

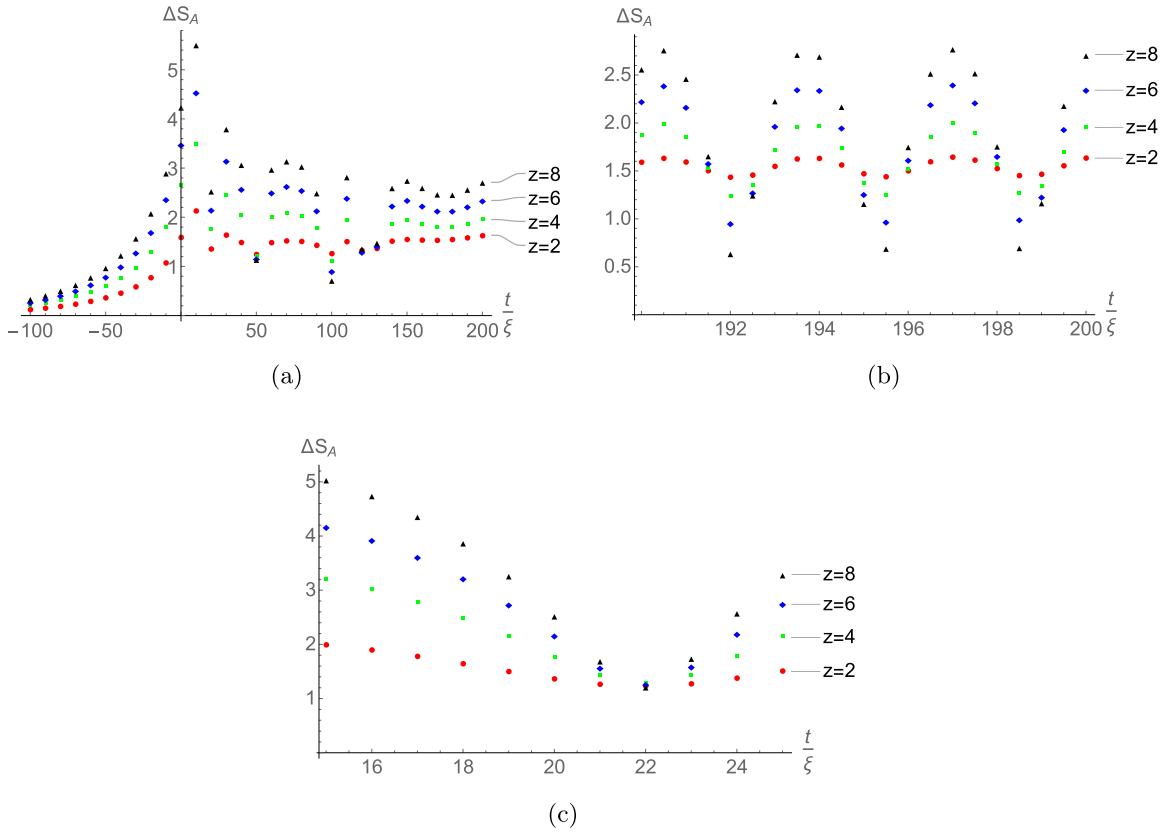

Figure 10. Time dependence of ΔS_A in the slow CCP for $z = 2, 4, 6, 8$ ($\xi = 10, \delta t = 1000, l = 1000$). (a) Comparison between $z = 2, 4, 6, 8 (-100 \leqslant t/\xi \leqslant 200)$. (b) Zoomed-in view of (a) ($190 \leqslant t/\xi \leqslant 200$) to see the oscillating feature clearly. (c) Zoomed-in view of (a) ($15 \leqslant t/\xi \leqslant 25$) to see a local minimum around $t/\xi \sim 2\xi_{\rm kz}/\xi \sim 20$.

of the magnitude of δt as explained in section 3.3. A main difference between the ECP and CCP is that ΔS_A in the CCP oscillates in t because the mass potential in the CCP at late times is nonzero. The period of oscillation in ΔS_A at late times can be inferred by (2.6) where $\omega_k = \sqrt{\frac{1}{\xi^2} + (2\sin[k/2])^{2z}}$ at late times. The period is $\frac{\pi}{\omega_k}$ and it is estimated with $k = 0$ because the dominant contribution at late times comes from small $k \sim 0$. (See, for example, the entropy density plots: figures 12 and 14. One can check that the entropy density $s(k)$ in the sudden quench is maximum at $k = 0$.) Therefore, the period is $\pi\xi$ and does not depend on z.

4.3.2. (Cf3) and (Cs3). As shown in figure 7, the time scale at which the significant subsystem size-dependence of ΔS_A in the fast CCP with $z = 2$ occurs is later than $t \sim l/2$[18] (the property (Cf3)). In the CCP, we also confirmed this delayed t_c for $z = 4, 6, 8$. The time scale $t \sim l/2$ is the one of ΔS_A in the fast CCP with $z = 1$ and can be explained by the maximum group velocity of the quasiparticles. If we can use the quasiparticle picture to interpret the time scale of ΔS_A in the fast CCP with $z = 2$,

[18] In the slow CCP, t_c for $z = 2$ is delayed compared with $z = 1$ case. However, it is not clear that the quasiparticle picture is valid to interpret t_c even for $z = 1$ [13].

J. Stat. Mech. (2019) 093104

delay of the time scale with $z=2$ can be interpreted by small contribution of the fast quasiparticles to ΔS_A as explained in section 3.3.

4.3.3. (Cf4) and (Cs4). As z increases, the long-range interaction in the Lifshitz theories with $z>1$ seems to make the amplitude of oscillation in ΔS_A larger.

4.3.4. (Cf2,5) and (Cs2,5). We do not have a good understanding on why the time scales of the first local minimum of ΔS_A is around 2ξ and $2\xi_{\rm kz}$ independently of z for fast and slow CCP respectively. This time scale is identified in [13] for $z=1$ case.

5. Delayed time scale: quasiparticle picture for $z>1$

As in the examples in the previous sections, we found that the critical time t_c for $z\geqslant 2$ is delayed compared with the case $z=1$, i.e.

$$t_c(z\geqslant 2) > t_c(z=1). \tag{5.1}$$

In this section, we interpret this by using the the quasiparticle formula of entanglement entropy in the sudden quench [21, 22]. We show examples of t_c such that

$$t_c \gg \frac{l}{2|v_{\rm max}|}, \tag{5.2}$$

by using the quasiparticle formula in the sudden quench for $z\geqslant 2$. This result supports our interpretation that (5.1), in fact, should be understood as

$$t_c \gg t_{\rm kz} + \frac{l}{2|v_{\rm max}|}, \tag{5.3}$$

as we explained in (3.5) and (3.8) in the fast and slow ECP and fast CCP for $z\geqslant 2$. For the fast ECP and CCP case, $t_{\rm kz}\sim 0$. For the slow ECP, $t_{\rm kz}$ is non-zero. See footnote 14 for more details. In the following section, for example, we focus on $z=2$ case.

5.1. Review of the quasiparticle formula

We explained a basic idea of the quasiparticle picture in section 3.3. This idea can be generalized to the case $z>1$ [40] and $0<z<1$ [41, 48]. We again consider a one-dimensional system with a subsystem A of length l under a sudden quench, where the mass potential changes at $t=0$ from the initial mass m_0 to the final mass m_f.

The idea of $z=1$ case still applies to $z>1$ case and the explanation in figure 6 also works for $z>1$. Namely in early time regime $t<\bar{t}:=\frac{l}{2|v_k|}$ (yellow area) the quasiparticle pairs created in the length of $2|v_k|t$ contribute, while in late time regime $t>\bar{t}$ (green area) the quasiparticle pairs created in the length of l contribute. However, the difference between $z=1$ and $z>1$ is in the value of maximum group velocity. This is not shown in figure 6, which describes the situation at some fixed v_k.

In order to explain the delayed critical time, we need to consider the quasiparticle picture in more detail, quantitatively. The group velocity v_k is a function of k and the created quasiparticle entropy density $s(k)$, which we will explain later, is also a

J. Stat. Mech. (2019) 093104

function of k. Thus, in total, the entanglement entropy created by the quasiparticle pairs ($\Delta S_A^{\rm q}(t)$) reads [21, 22]:

$$\Delta S_A^{\rm q}(t) = t\int_{2|v_k|t<l} {\rm d}k s(k) 2|v_k| + l\int_{2|v_k|t>l} {\rm d}k s(k), \tag{5.4}$$

where $k\in[-\pi,\pi]$, and the superscript q stands for the 'quasiparticle formula' to emphasize the difference with $\Delta S_A(t)$ by the 'correlator method'. The first term comes from the yellow area, and the second term comes from the green area in figure 6. Note that $\Delta S_A^{\rm q}$ starts depending on the subsystem size l after $t=\frac{l}{2|v_{\max}|}$ because the second term in (5.4) is zero before $t=\frac{l}{2|v_{\max}|}$, where $v_{\max}$ is the maximum group velocity of v_k. At fixed t, we can choose large but finite l such that the second term in (5.4) becomes zero. Based on this property, we define $\Delta S_A^{\rm q}(t)|_{l\to\infty}$ as

$$\Delta S_A^{\rm q}(t)|_{l\to\infty} := t\int_{-\pi}^{\pi} {\rm d}k s(k) 2|v_k|. \tag{5.5}$$

We also assume that the entropy density $s(k)$ for the entanglement entropy (5.4) is equivalent to the thermodynamic entropy density which is computed from a density matrix $\rho_{\rm GGE}$ of a generalized Gibbs ensemble [5, 22] as

$$\rho_{\rm GGE} = Z^{-1}{\rm e}^{-l\int\frac{{\rm d}k}{2\pi}\lambda_k\hat{n}_k}, \tag{5.6}$$

where Z is a normalization factor, λ_k are Lagrange multiplies, and $\hat{n}_k=a_k^\dagger a_k$ are number operators for Hamiltonian after the quench. This assumption implies the entanglement entropy becomes the thermodynamic entropy at late time limit. Requiring the conservation of the expectation value of the number operator between the initial state and the generalized Gibbs ensemble at late times, ${\rm Tr}\,[\hat{n}_k\rho_{\rm GGE}]=\langle 0|\hat{n}_k|0\rangle$, where $|0\rangle$ is the initial ground state of Hamiltonian before the quench, we obtain

$${\rm e}^{\lambda_k} = 1+\frac{1}{\langle 0|\hat{n}_k|0\rangle}. \tag{5.7}$$

In free scalar theories in the sudden quench, the explicit form of $s(k)$ is [5, 22]

$$s(k) = \frac{1}{2\pi}\left[(n_k+1)\log(n_k+1)-n_k\log(n_k)\right], \tag{5.8}$$

$$n_k := \langle 0|\hat{n}_k|0\rangle = \frac{1}{4}\left(\frac{\omega_k}{\omega_{0,k}}+\frac{\omega_{0,k}}{\omega_k}\right)-\frac{1}{2}, \tag{5.9}$$

where we use the dispersion relations $\omega_{0,k}$ before the quench and ω_k after the quench of the Lifshitz theories as

$$\omega_{0,k} = \sqrt{m_0^2+(2\sin[k/2])^{2z}},\quad \omega_k = \sqrt{m_f^2+(2\sin[k/2])^{2z}}. \tag{5.10}$$

The group velocity v_k after the quench in these theories is

$$v_k := \frac{{\rm d}\omega_k}{{\rm d}k} = \frac{z\cos[k/2]\,(2\sin[k/2])^{2z-1}}{\sqrt{m_f^2+(2\sin[k/2])^{2z}}}. \tag{5.11}$$

J. Stat. Mech. (2019) 093104

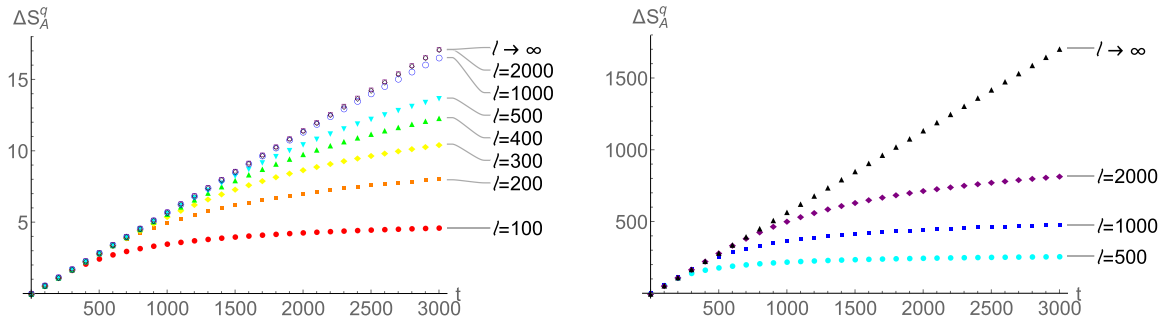

Figure 11. The change of the entanglement entropy $\Delta S_A^{\rm q}$ (5.4) in the sudden quench for $z=2$ and $m_f=10^{-6}$. The change $\Delta S_A^{\rm q}$ for $l\to\infty$ is (5.5). (a) $m_0=10^{-2}$. (b) $m_0=1$.

With these expressions (5.8)–(5.11), one can compute (5.4) explicitly.

5.2. Examples

Entanglement entropy with $z>1$ by the quasiparticle picture was also studied in [40], where $m_0=1$ and $m_f=0,2^z$ are considered. Compared with [40], we are interested in small $m_0\ll 1$ because i) it corresponds to the field theory limit, i.e. $\xi\gg 1$ where ξ is measured by the lattice spacing; ii) it corresponds to our model in section 3.1. Furthermore, our analysis is extended to explain the delayed t_c, which is complementary to [40].

For example, let us consier $\Delta S_A^{\rm q}$ for $z=2$. We choose a small but nonzero value of $m_f=10^{-6}$ to avoid the divergence of n_k at $k=0$. Figure 11 plots $\Delta S_A^{\rm q}(t)$ in (5.4) for various subsystem sizes $l=100,200,300,400,500,1000,2000$. Figure 11(a) is for the initial mass $m_0=0.01$, and figure 11(b) is for $m_0=1$.

Note that figure 11(a) should be compared with figure 2(a) because the sudden quench is a limit of the fast ECP. For both plots, the initial mass is the same, and the finial mass is almost zero. However, figure 11(a) is computed by the quasiparticle picture (5.4) while figure 2(a) is computed by the correlator method. (The horizontal time axis is scaled by ξ in figure 2(a).) Their significant subsystem size-dependences agree with each other very well[19].

5.3. Why delayed critical time?

Let us now turn to our main question: why is the critical time t_c delayed for $z=2$ compared with the $z=1$ case? To answer the question, we first revisit the argument for $z=1$ (See (3.3)). In order to determine t_c, we use the maximum group velocity $v_{\rm max}$ in (3.3). For the massless quasiparticle with $z=1$, we obtain $v_{\rm max}=1$ and $t_c\sim\frac{l}{2|v_{\rm max}|}=\frac{l}{2}$.

To investigate this property in more detail, let us rewrite (5.4) as

[19] The numerical values of the entanglement entropy is slightly different. Roughly speaking,

$$\Delta S_A(\text{figure 2(a)})\geqslant\Delta S_A^{\rm q}(\text{figure 11(a)}). \tag{5.12}$$

This is because the mass ratio m_0/m_f is too big as argued in [40]. (See figures 6 and 8 in [40].)

J. Stat. Mech. (2019) 093104

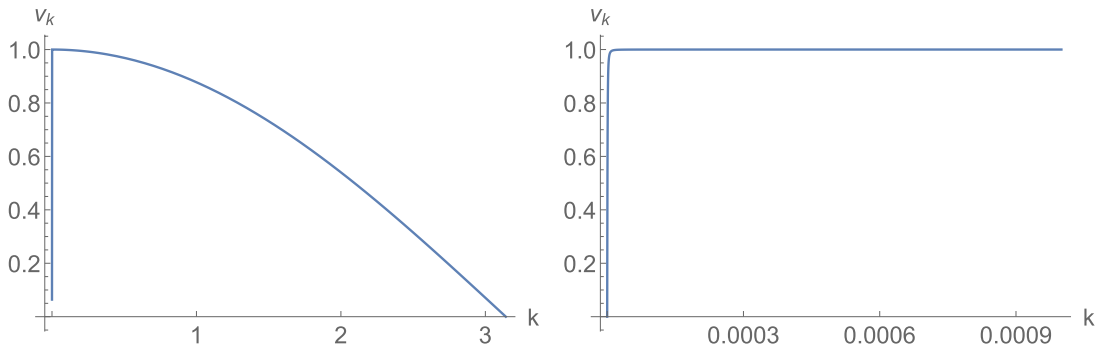

(a)

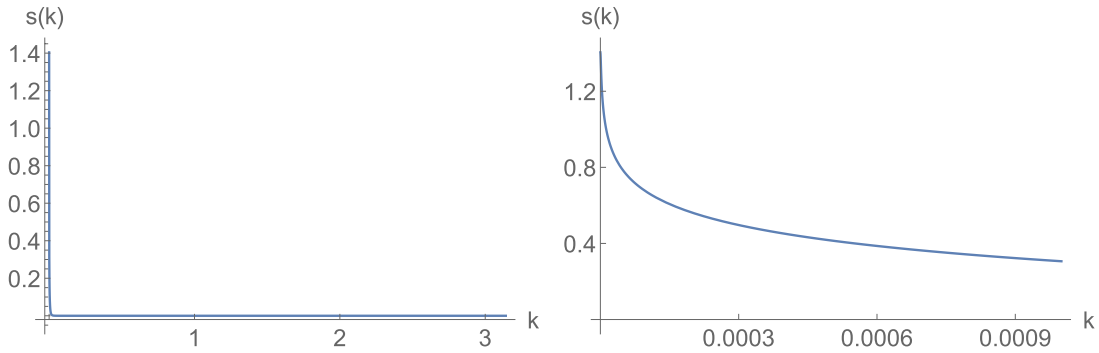

(b)

Figure 12. Group velocity v_k and entropy density $s(k)$ for $z=1$, $m_0=10^{-2}$, and $m_f=10^{-6}$. (a) Group velocity v_k. The right panel is a zoomed-in view of the left panel near $k=0$. (b) Entropy density $s(k)$. The right panel is a zoomed-in view of the left panel near $k=0$.

$$\Delta S_A^{\rm q}(t) = t\int_{-\pi}^{\pi} {\rm d}k s(k) 2|v_k| - \int_{2|v_k|t>l} {\rm d}k (2|v_k|t-l)s(k). \tag{5.13}$$

Here, the first term in (5.13) does not depend on l. The change $\Delta S_A^{\rm q}$ depends on l after $t=\frac{l}{2|v_{\rm max}|}$ because of the second term in (5.13). Only after $t\sim\frac{l}{2|v_{\rm max}|}$, the quasiparticle pairs with $v_k\sim v_{\rm max}$ starts contributing. However, in this case, the factor $(2|v_k|t-l)$ in the integrand of the second term is small. Unless $s(k)$ is large enough the l-dependence due to the second term will be negligible near $t\sim\frac{l}{2|v_{\rm max}|}$ even though it is non-zero. Thus, we find that a naive argument for $z=1$ needs to be revisited.

5.3.1. $z=1$ case. In figure 12, we make plots of (5.8) and (5.11) for $s(k)$ and v_k respectively, where $m_0=10^{-2}$ and $m_f=10^{-6}$. The group velocity v_k is maximum ($v_{\rm max}\sim 1$) near $k\sim 0$ (figure 12(a)). Near $k\sim 0$, $s(k)$ is dominant, which makes the integrand of the second term of (5.13) big enough as we suspected. It explains $t_c\sim\frac{l}{2}$ for $z=1$.

5.3.2. $z=2$ case. Let us turn to the $z=2$ case. Figure 13 shows the group velocity v_k for $m_0=10^{-2}$. Unlike the $z=1$ case, $|v_k|$ at $|k|\sim 1.6$ is maximum, which is away

J. Stat. Mech. (2019) 093104

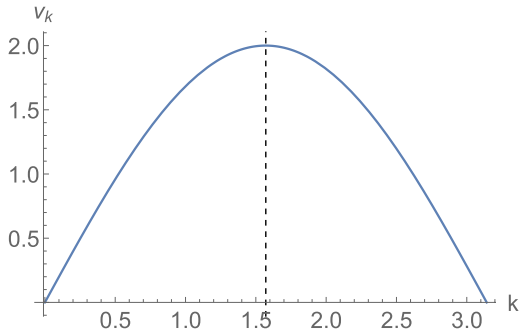

Figure 13. Group velocity v_k for $z = 2$ and the final mass $m_f = 10^{-6}$. It is independent of the initial mass m_0. The group velocity v_k at $k = k^* \approx 1.6$ is maximum.

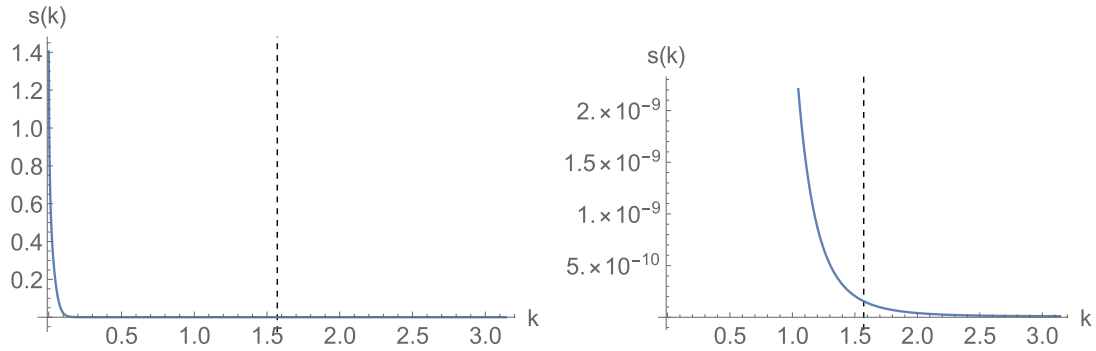

(a)

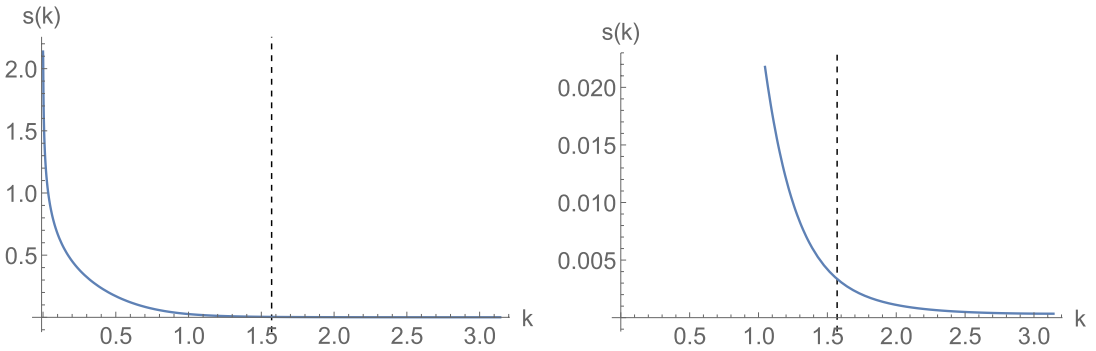

(b)

Figure 14. The plot of entropy density $s(k)$ for $z = 2$ and $m_f = 10^{-6}$. The dashed lines represent the momentum k^*. (a) $m_0 = 10^{-2}$. The right panel is a zoomed-in view of the left panel to show the value of $s(k^*)$. (b) $m_0 = 1$. The right panel is a zoomed-in view of the left panel to show the value of $s(k^*)$.

from $k = 0$. Figure 14(a) shows the quasiparticle pair entropy density $s(k)$ of the fast quasiparticles around $|k| \sim 1.6$ is much smaller than the one of the slow quasiparticles around $k \sim 0$. The smallness of $s(k)$ of the fast quasiparticles makes their contribution to the entanglement entropy small (the integrand of the second term of (5.13) is small).

J. Stat. Mech. (2019) 093104

Consequently, t_c becomes delayed compared with $t = \frac{l}{2|v_{\max}|} \sim \frac{l}{4}$. Thus, for example, $t_c > 3000$ for $l = 1000$ from figure 11(a), i.e.

$$t_c(m_0 = 10^{-2}, l = 2000) > 3000 > \frac{l}{4} = 250. \tag{5.14}$$

For another comparison, we show the entropy density $s(k)$ for $m_0 = 1$ in figure 14(b). The entropy density $s(k)$ for the fast quasiparticles with $m_0 = 1$ is larger than that with $m_0 = 10^{-2}$. The group velocity of quasiparticles in the sudden quench with $m_0 = 1$ is the same as the one with $m_0 = 10^{-2}$ as in figure 13. Thus, we expect t_c to be less delayed compared with the $m = 10^{-2}$ case. Indeed, it turns out to be the case. For example, $t_c \sim 800$ for $l = 2000$ from figure 11(b), i.e.

$$t_c(m_0 = 1, l = 2000) \sim 800 > \frac{l}{4} = 250, \tag{5.15}$$

which corresponds to the case (3.6) because

$$t_c(m_0 = 1, l = 2000) \sim 800 < \frac{l}{2} = 1000. \tag{5.16}$$

In short, in this case, t_c is not delayed so much compared with $z = 1$ case, but still delayed compared with $\frac{l}{2|v_{\max}|}$.

5.3.3. $z > 2$ case. The qualitative feature of v_k and $s(k)$ for $z > 2$ are the same as the $z = 2$ case. The peak of v_k is more shifted to the right as z increases. Thus t_c is delayed by the same reason. The general behavior of v_k can be understood by (5.11). If we take $m_f = 0$ then, the dependence of $\sin[k/2]$ will disappear only for $z = 1$.

In short, in the quasiparticle picture the delayed t_c can be explained by the small contribution of the fast quasiparticles to the entanglement entropy.

6. Conclusions

We have studied the time evolution of the entanglement entropy in the free Lifshitz scalar theories with the time-dependent mass by the correlator method on one-dimensional spacial lattice. The mass potentials are smooth functions of time (ECP or CCP), and the initial ground states evolve in time by the time-dependent Hamiltonians.

Some important observations and comments from our computations are as follows.

1. At early times: for both ECP and CCP, the entanglement entropy is subsystem size independent. It can be understood intuitively by the quasiparticle picture as shown in figure 6.
2. The (intermediate) critical time: from a naive application of the quasiparticle picture *only* by the fast quasiparticle, we expect the critical time t_c for the significant l-dependence in the sudden quench to become $t_c \sim \frac{l}{2|v_{\max}|}$. It works for $z = 1$ in the sudden quench, however, for the fast and slow ECP and the fast CCP with $z > 1$, we have found that it is possible

J. Stat. Mech. (2019) 093104

$$t_c \gg t_{\rm kz} + \frac{l}{2|v_{\rm max}|}, \tag{6.1}$$

where $t_{\rm kz}$ is the Kibble–Zurek time, the time scale when the quasiparticle pairs with $k \sim 0$ are created. For the Fast ECP and CCP case, $t_{\rm kz} \sim 0$. We have explained that, by the quasiparticle formula in the sudden quench, it can be interpreted by the negligible contribution of the fast quasiparticles due to its small entropy density. Indeed, the dominant contribution comes from the slow quasiparticles. (For $z = 1$ case, the entropy density is large for the fast quasiparticles, which is why the *only* fast particle approximation works for $z = 1$.) In addition, t_c increases as the subsystem sizes increase.

3. At late times: for the ECP, the entanglement entropy is slowly increasing. For the CCP with the final mass m_f, the entanglement entropy is oscillating with a period $\sim \pi/m_f$, which can be understood by the dominant contribution by the slow quasiparticles with the momentum $k \sim 0$.

4. z-dependence: the entanglement entropy increases as z increases, which can be interpreted as the effect of the long-range interactions due to the higher derivative ∂_x^z in (2.1).

5. The time scale for the first local minimum of the entanglement entropy in the CCP case: it is around 2ξ for the fast CCP and $2\xi_{\rm kz}$ for the slow CCP *independently* of z.

Even though we have found that the quasiparticle picture is successful in understanding some of our results qualitatively for $z > 1$ as well as $z = 1$, note that it is a picture for the *sudden* quench. For a slow change of the mass potential or for a small final mass (see footnote 19), there will be quantitative differences from the quasiparticle picture. Therefore, the property items 1 and 2 can be explained well by the quasiparticle picture, but it is not easy to determine precise t_c by that picture. It is also not easy to determine the value of t_c from our numerical correlator method; we first need to define some criteria for the significant deviation due to the subsystem size. Some of our results cannot be explained even qualitatively by that picture. For example, the nonlinear behavior of ΔS_A with large z in figure 2 cannot be explained. It will be interesting to understand the z-dependence of this nonlinear behavior[20] as well as more detailed understanding of item 4. Furthermore, it will be also interesting to consider the entanglement entropy at a limit $z \to \infty$ for understanding the effect of large z.

Based on the argument in item 3, we may say that the entanglement entropy in our ECP does not oscillate at late times because $m_f \sim 0$. If we considered the ECP with a finite m_f, we would have observed an oscillation. It will be interesting to check this expectation by the correlator method. The last item 5 is very interesting since it shows a universal property independent of z. Even though our results are numerical, it seems very robust. We do not have a good understanding on it yet, and leave it as a future work.

[20] See also discussion of the z-dependence of entanglement entropy at early times in [40].

J. Stat. Mech. (2019) 093104

Acknowledgment

We would like to thank Kyoung-Bum Huh, Hyun-Sik Jeong, Chang-Woo Ji, and Ali Mollabashi for fruitful discussions. The work of K-Y Kim, M Nishida, and M-S Seo was supported by Basic Science Research Program through the National Research Foundation of Korea (NRF) funded by the Ministry of Science, ICT & Future Planning (NRF-2017R1A2B4004810) and GIST Research Institute (GRI) grant funded by the GIST in 2019. M Nozaki is supported by JSPS Grant-in-Aid for Scientific Research (Wakate) No. 19K14724. The work of M Nozaki is supported by RIKEN iTHEMS Program. The work of M Nozaki and AT were the RIKEN Special Postdoctoral Researcher program. K-Y Kim, M Nishida, and M-S Seo also would like to thank the APCTP (Asia-Pacific Center for Theoretical Physics) focus program, 'Holography and geometry of quantum entanglement' in Seoul, Korea for the hospitality during our visit, where part of this work was done.

References

[1] Gogolin C and Eisert J 2016 Equilibration, thermalisation, and the emergence of statistical mechanics in closed quantum systems *Rep. Prog. Phys.* **79** 056001
[2] Page D N 2005 Hawking radiation and black hole thermodynamics *New J. Phys.* **7** 203
[3] Calabrese P and Cardy J L 2006 Time-dependence of correlation functions following a quantum quench *Phys. Rev. Lett.* **96** 136801
[4] Calabrese P, Essler F H L and Mussardo G 2016 Introduction to 'quantum integrability in out of equilibrium systems' *J. Stat. Mech.* 064001
[5] Calabrese P and Cardy J 2007 Quantum quenches in extended systems *J. Stat. Mech.* P06008
[6] Chandran A, Erez A, Gubser S S and Sondhi S L 2012 Kibble–Zurek problem: universality and the scaling limit *Phys. Rev.* B **86**
[7] Das S R, Galante D A and Myers R C 2014 Universal scaling in fast quantum quenches in conformal field theories *Phys. Rev. Lett.* **112** 171601
[8] Das S R, Galante D A and Myers R C 2015 Universality in fast quantum quenches *J. High Energy Phys.* JHEP02(2015)167
[9] Das S R, Galante D A and Myers R C 2015 Smooth and fast versus instantaneous quenches in quantum field theory *J. High Energy Phys.* JHEP08(2015)073
[10] Das S R, Galante D A and Myers R C 2016 Quantum quenches in free field theory: universal scaling at any rate *J. High Energy Phys.* JHEP05(2016)164
[11] Caputa P, Das S R, Nozaki M and Tomiya A 2017 Quantum quench and scaling of entanglement entropy *Phys. Lett.* B **772** 53–7
[12] Alves D W F and Camilo G 2019 Momentum-space entanglement after smooth quenches *Eur. Phys. J.* C **79** 48
[13] Nishida M, Nozaki M, Sugimoto Y and Tomiya A 2017 Entanglement spreading and oscillation (arXiv:1712.09899)
[14] Alves D W F and Camilo G 2018 Evolution of complexity following a quantum quench in free field theory *J. High Energy Phys.* JHEP06(2018)029
[15] Camargo H A, Caputa P, Das D, Heller M P and Jefferson R 2018 Complexity as a novel probe of quantum quenches: universal scalings and purifications (arXiv:1807.07075)
[16] Fujita H, Nishida M, Nozaki M and Sugimoto Y 2018 Dynamics of logarithmic negativity and mutual information in smooth quenches (arXiv:1812.06258)
[17] Mohammadi Mozaffar M R and Mollabashi A 2019 Universal scaling in fast quenches near Lifshitz-like fixed points (arXiv:1906.07017)
[18] Peschel I and Eisler V 2009 Reduced density matrices and entanglement entropy in free lattice models *J. Phys. A: Math. Theor.* **42** 504003
[19] Calabrese P and Cardy J L 2005 Evolution of entanglement entropy in one-dimensional systems *J. Stat. Mech.* P04010

J. Stat. Mech. (2019) 093104

[20] Cotler J S, Hertzberg M P, Mezei M and Mueller M T 2016 Entanglement growth after a global quench in free scalar field theory *J. High Energy Phys.* JHEP11(2016)166
[21] Alba V and Calabrese P 2017 Entanglement and thermodynamics after a quantum quench in integrable systems *PNAS* **114** 7947
[22] Alba V and Calabrese P 2018 Entanglement dynamics after quantum quenches in generic integrable systems *SciPost Phys.* **4** 017
[23] Lifshitz E 1941 On the theory of second-order phase transitions I & II *Zh. Eksp. Teor. Fiz* **11** 255, 269
[24] Hornreich R M, Luban M and Shtrikman S 1975 Critical behavior at the onset of $\vec{k}$ instability on the λ line *Phys. Rev. Lett.* **35** 1678–81
[25] Horava P 2009 Quantum gravity at a Lifshitz point *Phys. Rev.* D **79** 084008
[26] Solodukhin S N 2010 Entanglement entropy in non-relativistic field theories *J. High Energy Phys.* JHEP04(2010)101
[27] Keranen V, Keski-Vakkuri E and Thorlacius L 2012 Thermalization and entanglement following a non-relativistic holographic quench *Phys. Rev.* D **85** 026005
[28] Fischetti S and Marolf D 2014 Complex entangling surfaces for AdS and Lifshitz black holes? *Class. Quantum Grav.* **31** 214005
[29] Hosseini S M and Vliz-Osorio L 2016 Entanglement and mutual information in two-dimensional nonrelativistic field theories *Phys. Rev.* D **93** 026010
[30] Gentle S A and Keeler C 2016 On the reconstruction of Lifshitz spacetimes *J. High Energy Phys.* JHEP03(2016)195
[31] Zhou T, Chen X, Faulkner T and Fradkin E 2016 Entanglement entropy and mutual information of circular entangling surfaces in the 2 + 1-dimensional quantum Lifshitz model *J. Stat. Mech.* 093101
[32] Kusuki Y, Takayanagi T and Umemoto K 2017 Holographic entanglement entropy on generic time slices *J. High Energy Phys.* JHEP06(2017)021
[33] Gentle S A and Vandoren S 2018 Lifshitz entanglement entropy from holographic cMERA *J. High Energy Phys.* JHEP07(2018)013
[34] Mohammadi Mozaffar M R and Mollabashi A 2018 Logarithmic negativity in Lifshitz harmonic models *J. Stat. Mech.* 053113
[35] Wen Q 2019 Towards the generalized gravitational entropy for spacetimes with non-Lorentz invariant duals *J. High Energy Phys.* JHEP01(2019)220
[36] Mohammadi Mozaffar M R and Mollabashi A 2017 Entanglement in Lifshitz-type quantum field theories *J. High Energy Phys.* JHEP07(2017)120
[37] He T, Magan J M and Vandoren S 2017 Entanglement entropy in Lifshitz theories *SciPost Phys.* **3** 034
[38] Chen X, Fradkin E and Witczak-Krempa W 2017 Quantum spin chains with multiple dynamics *Phys. Rev.* B **96** 180402
[39] Chen X, Fradkin E and Witczak-Krempa W 2017 Gapless quantum spin chains: multiple dynamics and conformal wavefunctions *J. Phys. A: Math. Theor.* **50** 464002
[40] Mohammadi Mozaffar M R and Mollabashi A 2019 Entanglement Evolution in Lifshitz-type Scalar Theories *J. High Energy Phys.* JHEP01(2019)137
[41] Ghasemi Nezhadhaghighi M and Rajabpour M A 2014 Entanglement dynamics in short and long-range harmonic oscillators *Phys. Rev.* B **90** 205438
[42] Peschel I 2003 Calculation of reduced density matrices from correlation functions *J. Phys. A: Math. Gen.* **36** L205
[43] Casini H and Huerta M 2009 Entanglement entropy in free quantum field theory *J. Phys. A: Math. Theor.* **42** 504007
[44] Fagotti M and Calabrese P 2008 Evolution of entanglement entropy following a quantum quench: analytic results for the x y chain in a transverse magnetic field *Phys. Rev.* A **78** 010306
[45] Bernard C W and Duncan A 1977 Regularization and renormalization of quantum field theory in curved space-time *Ann. Phys.* **107** 201
[46] Gritsev V and Polkovnikov A 2009 Universal dynamics near quantum critical points *Understanding Quantum Phase Transitions* ed L D Carr (Boca Raton, FL: Taylor & Francis)
[47] Coser A, Tonni E and Calabrese P 2014 Entanglement negativity after a global quantum quench *J. Stat. Mech.* P12017
[48] Rajabpour M A and Sotiriadis S 2015 Quantum quench in long-range field theories *Phys. Rev.* B **91** 045131

J. Stat. Mech. (2019) 093104